Magnetic and transport properties of UBi2 and USb2 single crystals

Ryszard Wawryk

Magnetic and transport properties of UBi2 and USb2 single crystals

Journal:	*Philosophical Magazine & Philosophical Magazine Letters*
Manuscript ID:	TPHM-05-Jun-0297.R2
Journal Selection:	Philosophical Magazine
Date Submitted by the Author:	29-Nov-2005
Complete List of Authors:	Wawryk, Ryszard; Institute of Low Temperature and Structure Research Polish Academy of Sciences
Keywords:	thermoelectric power, anisotropy, electronic transport, magnetic properties, resistivity
Keywords (user supplied):	Uranium dipnictides; Magnetic susceptibility; Resistivity; Thermoelectric power

Magnetic and transport properties of UBi_2 and USb_2 single crystals

RYSZARD WAWRYK

Electronic Transport Department, W. Trzebiatowski Institute of Low Temperature and Structure Research, Polish Academy of Sciences, 50-950 Wrocław 2, PO Box 1410, Poland

ABSTRACT

Thermoelectric power, $S(T)$, of USb_2 and UBi_2 that are tetragonal, uniaxial antiferromagnets below T_N = 202 K and 180.8 K, respectively, have been examined between 0.4 K and 300 K. The $S(T)$ dependencies, up to now known above 70 K for USb_2 and unknown for UBi_2, are along the *a*-axis positive for both compounds in the whole examined temperature range. The $S(T)$ data for the *c*-axis (the easy magnetisation axis) are positive near the room temperature for USb_2 and UBi_2 and becomes negative below 120 K and 170 K, respectively, with two very deep minima in $S(T)$ dependence for USb_2. In the latter compound the Fermi surface, known from literature, is compose of the only cylindrical sheets that are slightly corrugated and parallel to the *c*-axis. UBi_2, the Fermi surface of which is composed of one spherical and two cylindrical sheets shows the corresponding minima to be less pronounced than those in USb_2. Having in disposal the highest purity single crystals in comparison to those for which the resistivity, $\rho(T)$, has been reported in literature up to now, the $\rho(T)$ anisotropy could be re-examined for these two systems. Magnon and phonon contributions to their total electrical resistivity have been determined and critical fluctuation behaviour of the resistivity near T_N for both dipnictides has also been analysed. Although the magnetic susceptibilities of UBi_2 and USb_2 reveal a similarity, their transport properties are significantly different due to the difference in the Fermi surface topology.

Keywords: Uranium dipnictides; Magnetic susceptibility; Resistivity; Thermoelectric power

§ 1. INTRODUCTION

The UBi_2 and USb_2 compounds belong to group of the uranium dipnictides UX_2 (X=P, As, Sb, Bi) - they were, and are still intensively investigated due to their unusual transport properties. The magnetic properties of UBi_2 and USb_2 are described in Refs. [1] – [5], whereas the limited transport properties are presented in Refs. [6, 7, 8]. The crystal structure and the Fermi surface [9] of both compounds are well defined. Therefore the aim of this work is to show how their features are reflected in the electrical transport coefficients.

UBi_2 and USb_2 crystallise in a tetragonal structure belonging to the anti-Cu_2Sb-type with either P4/nmm or $\mathbf{D}_{4h}^{7}$ space group. The unit cell contains two formula units and the ratio of unit cell parameters c/a equals to 2.004 and 2.044 for UBi_2 and USb_2, respectively. The neutron-diffraction study [3] showed that below the Néel temperature they order antiferromagnetically, along the c-axis, with alternating ferromagnetic sheets in the sequences (↑↓↓↑) for USb_2 and (↑↓) for UBi_2. Such an ordering results in the magnetic unit cell of USb_2, which is twice the chemical unit cell along the c-axis, while the magnetic and chemical unit cells of UBi_2 are of the same size. Hence the magnetic Brillouin zone for UBi_2 being fairly flat is the same as that of the chemical one. The ratio of the length k_c along [001] to the length k_a along [100] in the magnetic Brillouin zone of USb_2 and UBi_2 is 0.24 and 0.5, respectively.

The de Haas-van Alphen and Shubnikov-de Haas experiments have allowed for constructing the Fermi surface for UBi_2 and USb_2 in the ordered state [9]. It consists of one spherical (α) and two cylindrical (β) sheets in UBi_2 and entirely cylindrical sheets in USb_2. The magnetic Brillouin zone in USb_2 consists of one of each cylindrical sheets (α) and (δ), and two of each of cylindrical sheets (ε) and (γ). The Fermi surfaces of UBi_2 are the same in the paramagnetic and antiferromagnetic states. In the case of USb_2 the paramagnetic Fermi surfaces are related to those in UBi_2, because the Brillouin zone in USb_2 is almost the same as that in UBi_2 and it is occupied by similar number of electrons. Thus, in the paramagnetic state

the spherical sheet (α) in UBi_2 corresponds to the corrugated cylindrical one in USb_2 (see figures 24c and 25a in Ref. [9]) and the cylindrical sheet (β) in UBi_2 corresponds to the long ellipsoidal Fermi surfaces in USb_2 (see figure 24d in Ref. [9]). The latter crosses over the Brillouin zone boundary, forming another corrugated cylindrical and a small-pocket ellipsoidal Fermi surfaces.

The paramagnetic to antiferromagnetic transition in USb_2 increases the number of the Fermi surface sheets and enhances their quasi-two dimensionality, as discussed in Ref. [9].

An angle-resolved photoemission study in single crystal of USb_2 at 15 K [10] showed the dispersion of extremely narrow bands situated near the Fermi level. The natural linewidth is less than 10 meV. In the normal emission spectrum there is also a dispersion observed of about 10 meV, which indicates a 3D character in electronic structure of USb_2 in contrast to the earlier evidence [9]. These resonant photoemission measurements confirm the 5*f*-electron hybridisation with the conduction electrons.

This work presents results of measurements of the magnetic susceptibility $\chi(T)$, electrical resistivity $\rho(T)$, and thermoelectric power $S(T)$ down to 0.35 K, for UBi_2 and USb_2 single crystals. Their Fermi surfaces distinctly differ from each other.

We compare these data to those partially known from the literature and discuss the differences in the observed behaviours of USb_2 and UBi_2. These observed differences are related to the variation in the Fermi surface topology of these two compounds.

Deleted: ry

Deleted: The investigation of hyperfine interactions at the uranium sites in the antiferromagnetic state of uranium dipnictides was done using ^{238}U Mössbauer spectroscopy [11]. In UBi_2 the nuclear quadrupole interaction at ^{238}U is almost zero, whereas in USb_2 the sign of these interactions is negative. This suggests that the nuclear quadrupole interactions in both compounds are correlated with their magnetic structures.

Deleted: s

§ 2. Experimental details

USb_2 and UBi_2 single crystals were grown by the so called „molten metal solution" method [8]. They were grown in the form of plates with the dimensions of about 6×5×3 mm^3 along the *a*-, *b*-, and *c*- axes, respectively. For electrical resistivity and thermoelectric power examinations the specimens were cut out to the dimensions of about 4×0.5×0.5 mm^3 and 3×0.3×0.3 mm^3 for

carrying out the measurements along the *a*- and *c*- axes, respectively. The dc magnetic susceptibility in fields up to 5 T applied along the *c*-axis and in the temperature range 1.7 – 400 K was measured with a superconducting quantum interference device magnetometer (Quantum Design). The electrical resistivity at temperatures of 0.35 – 300 K was measured by a four point ac method. For the thermoelectric power measurements a modified set-up described in Ref. [11] has been used.

Deleted: 2

§ 3. RESULTS

3.1. *Magnetic susceptibility*

Magnetic susceptibility of a UBi_2 crystal, measured along the *c*-axis, shows the temperature dependence being typical for an antiferromagnet with a peak at T_N = 180.8 K (figure 1, see also Ref. [12]). In the paramagnetic state the modified Curie–Weiss law is fulfilled: $\chi(T) = \frac{\mathbf{N}\mu_{eff}^2}{3k_B(T+\Theta_p)} + \chi_0$, where N denotes the number of atoms in the unit cell, μ_{eff} is the effective magnetic moment, k_B is the Boltzmann constant, Θ_p is the paramagnetic Curie temperature, and χ_0 is the temperature independent paramagnetic contribution. The parameters are as follows: μ_{eff} = 3.36 μ_B, Θ_p = – 17 K, and $\chi_0 = 2.7\times 10^{-3}$ emu/mol. Obtained from the fit of above equation to experimental data the μ_{eff} value appears to be very close to that of 3.4 μ_B, reported in Ref. [2]. The determined μ_{eff} is however smaller from that of 3.62 μ_B or 3.58 μ_B expected for the free U^{+3} or U^{+4} ions, respectively.

Deleted: 3

[Insert figure 1 about here]

In the case of USb_2, the $\chi(T)$ dependence, measured along the *c*-axis, displays a sharp maximum yielding the Néel temperature of 202 K (figure 1, see also Ref. [13]). In this case, the modified Curie-Weiss law is obeyed in paramagnetic region for Θ_p = – 59 K and μ_{eff} = 3.32 μ_B.

Deleted: also

3.2. *Electrical resistivity*

The electrical resistivity of UBi_2 single crystals were carried out, in the *a* and *c* directions, for two different samples having different purity. They were (figure 2), obtained in different syntheses. The resistivity ratio $\rho_{300\ K}/\ \rho_{4.2\ K}$ = RR measured along the *a*-axis for the samples obtained in the first (1s) and second (2s) syntheses were 500 and 1110, respectively. The room temperature resistivity, $\rho_{300\ K}$, for both the (1s) and (2s) samples in the *a* direction was of 0.231 mΩ cm while in the *c* direction it was 3.88 mΩ cm. In the paramagnetic state the resistivity was found to be almost temperature independent, while that below T_N decreases rapidly in both directions with decreasing temperature.

[Insert figure 2 about here]

As seen in figure 2, distinct anisotropy in the temperature dependence of the resistivity is observed. Below T_N, the anisotropy ratio $(\rho_c - \rho_0)/(\rho_a - \rho_0)$ increases with decreasing temperature down to about 27 K. It achieves a value of about 2.7 times larger than that in the paramagnetic range (figure 3), and then it decreases at lower temperatures.

The temperature dependence of the anisotropy ratio $(\rho_c - \rho_0)/(\rho_a - \rho_0)$ differs from the results presented in Ref. [9], where the anisotropy ratio defined as ρ_c/ρ_a achieves a maximum value of about 800 at the temperature of circa 80 K. In the present work the $(\rho_c - \rho_0)/(\rho_a - \rho_0)$ ratio reaches at 27 K a maximum value of about 50 while the ρ_c/ρ_a ratio is not larger than about 100 (figure 3).

[Insert figure 3 about here]

This discrepancy in the anisotropy ratio probably arises from the difference in the sample purity. As mentioned above, the RR values for our samples in the *a* direction are 500 (1s) and 1110 (2s) compared to RR = 22 for the sample investigated by the authors of Ref. [9]. The RR values for the *c* direction in both cases were of the same order (i.e. 130 and 215 for our samples and 160 for the sample of Ref. [9]). Also the discrepancy in absolute values of the resistivity

Deleted: In the low temperature antiferromagnetic range there is visible a shallow valley in the $\chi(T)$ dependence for UBi_2 (the inset of figure 1). However, this valley is not as deep as that observed for USb_2 (see also Ref. [14]) or also for $UNiSb_2$ and $UPdSb_2$ there measured on the polycrystalline samples [15]. These minima in $\chi(T)$ curves, which occur at temperatures about 21 K and 50 K in UBi_2 and USb_2, respectively, may result from the crystal-field effects. In the ordered state, when the crystal field interaction is comparable with the exchange field interaction, anomalies in the $\chi(T)$ dependencies can occur. A crystal-field splitting (ground state is a doublet) of the order of the exchange interaction yields an anomalous temperature variation of the magnetic susceptibility as it was shown for CeSb and CeBi [16]. ¶

Deleted: the

appears; for example, the room temperature resistivity of our samples along the *a*- and *c*-axes are of 0.23 mΩ cm and 3.9 mΩ cm, while that for the samples from Ref. [9] these values are considerably different and amount to 60 mΩ cm and 3.4 × 10^4 mΩ cm, respectively. The samples differ mainly in the magnitudes of the residual resistivity, ρ_0.

According to the Matthiessen's rule the temperature dependence of the resistivity for an antiferromagnet can be written as follows:

$$\rho(T) = \rho_0 + a(T/\Theta)^{\mathbf{n}} \int_0^{\Theta/T} \frac{z^{\mathbf{n}}\mathbf{d}z}{(e^z - 1)(1 - e^{-z})} + bT(1 + 2T/\Delta)\exp\left(-\frac{\Delta}{T}\right) = \rho_0 + \rho_{\mathbf{ph}} + \rho_{\mathbf{m}}, \qquad (1)$$

where ρ_{ph} is approximated by the generalised Bloch-Grüneissen equation for electron-phonon scattering with n = 3 (similarly as for another uranium compounds, e.g. for $URhGa_5$ [14]). In Eq. (1) the ρ_m denotes the magnon component, Θ is the Debye temperature, Δ (= ε/k_B) is a gap in the magnons spectrum, and *a* and *b* are the fitting parameters. Whereas the third part of Eq. (1), which concerns the electron-magnon scattering, is limited to temperatures below $T_N/3$, the second part of Eq. (1) is valid in the whole temperature range (dashed line in figure 4).

[Insert figure 4 about here]

In figure 4 the fit of Eq. (1) to the experimental data is displayed by the solid line. The $\rho_m(T)$ equation was used previously for the fitting of the data in the case of the USb antiferromagnet [11].

The experimental $\rho(T)$ data of a USb_2 single crystal are displayed in figure 5. The results are similar to those obtained and described earlier in Refs. [7, 8] and [9], however a discrepancy in the anisotropy ratio is observed in comparison to the data of Ref. [9]. In the latter case a maximum value of about 90 is achieved in the ρ_c/ρ_a ratio at a temperature of circa 60 K, while for our sample this maximum value is found to be higher even than 190 and occurs at the temperature of 23 K (figure 3).

Deleted: 7

Deleted: 2

Deleted: the

Deleted: As mentioned above, USb_2 exhibits an antiferromagnetic ordering below T_N = 202 K.

In the paramagnetic state, near the critical temperature, $\rho(T)$ in the c direction in the limit of $0 \leq t \leq 0.04$ ($t = (T - T_N)/T_N$) can be expressed as that in Ref. [15]:

$$\rho(T) = A\ t^{1-\alpha} + B|\,t\,| + C \quad , \qquad (2)$$

where α is the critical exponent, A is the critical amplitude of the resistivity; B and C are the fitting parameters (first part of the solid curve 1 in figure 5). The exponent $(1 - \alpha)$ from Eq. (2) becomes ½ in the limit $0.04 \leq t \leq 0.12$ (second part). As seen from figure 5 (third part of the curve 1), formula (2) with $\alpha = 0.326$ gives a good fit to the experimental data at temperatures above 225 K. For the a-axis the resistivity between T_N and 260 K increases and then decreases slightly with increasing temperature to room temperatures.

[Insert figure 5 about here]

Below 70 K, for the $\rho(T)$ data taken in a similar way like in UBi_2 along the a-axis a sufficient approximation is given by Eq. (1) (curve 2 in the inset of figure 5). A good fit in the antiferromagnetic range is given by the equation: $\rho(T) = \rho_0 + \rho_{ph} + aT^{5/2}$ (dash-dotted line) [7]. For the c direction below $T_N/3$ Eq. (1) gives rather a poor fit.

The behaviours of critical resistivity for the UBi_2 and USb_2 single crystals in the a and c directions are presented in figure 6 as a function of the reduced temperature $t = (T - T_N)/T_N$. Using the classification from Ref. [16], the critical resistivity of a UBi_2 crystal in the a direction behaves like that for an antiferromagnetic semiconductor (figure 6a), while that along the c-axis as for an antiferromagnetic metal (figure 6b). This rule concerns USb_2 as well (figures 6c and 6d). The solid lines in figure 6 represent Eq. (2) fitted to the experimental data of the UBi_2 and USb_2 resistivities within the temperature limit $-0.08 \leq t \leq 0.08$ (for UBi_2 along the c-axis (figure 6b) this limit is equal to $-0.04 \leq t \leq 0.08$). The exponent $(1 - \alpha)$ becomes ½ at boundary marked by t_G.

[Insert figure 6 about here]

3.3. *Thermoelectric power*

The UBi_2 single crystals reveal a large anisotropy in the temperature dependence of the thermoelectric power $S(T)$ (see figure 7). Above the Néel temperature, $S(T)$ decreases and increases for the a and c directions, respectively. Below T_N, a few extremes in $S(T)$ are observed: for the a direction, after the change in slope at T_N, the two maxima in the temperature dependence of the thermoelectric power occur, the first one: ${}^{1a}S_{max}$ = 30.6 μV/K at ${}^{1a}T_{max}$ = 130 K and the second maximum ${}^{2a}S_{max}$ = 2.5 μV/K at ${}^{2a}T_{max}$ = 3.5 K.

[Insert figure 7 about here]

For the c-axis two minima in $S(T)$ exist: i.e. ${}^{1c}S_{min}$ = −5.9 μV/K and ${}^{2c}S_{min}$ = −1.0 μV/K at ${}^{1c}T_{min}$ and ${}^{2c}T_{min}$ of 103 K and 13.5 K, respectively. The $S(T)$ curve for UBi_2 along the c direction changes its sign thrice, namely at temperatures: 33.5 K, 38 K, and 166 K.

The $S(T)$ dependencies for a USb_2 single crystal along the a and c directions are presented in figure 8. They are similar to the results presented in Refs. [8, 17] along the a direction in the temperature range 50 – 300 K and are similar to the results of Ref. [17] in the c direction in the temperature range 75 – 300 K. However in the latter case they differ in absolute values of S at lower temperatures. In general, the thermoelectric power for USb_2 differs from that of UBi_2, particularly in that taken along the a-axis. However, a maximum of ${}^{a}S_{max}$ = 14.2 μV/K in the antiferromagnetic range exists, but it is single and appears at ${}^{a}T_{max}$ = 25 K. This maximum can be explained if we assume that the total thermoelectric power is a sum of the two components: the diffusion one, S_d, that increases linearly with temperature and the magnon/phonon-drag one, S_g, which is pieaked. The phonon-drag thermoelectric power depends on temperature as T^3 before the maximum of the peak and as $1/T$ on the right hand side of S_{max} [18]. The solid curve 1 (the inset on the left hand side in figure 8) presents the equation: $S(T) = S_d + S_g = aT + b/T$ fitted to the experimental data of $S(T)$ within the temperature range 25 – 90 K. The S_d (straight line 2) was calculated from the above equation,

Deleted: 20

Deleted: 20

Deleted: c

Deleted: 21

whereas the S_g (curve 3) was estimated as the difference between the experimental data and diffusion contribution. The maximum of S_g appears at $T^* = 7.5$ K.

Similarly like for UBi_2, $S(T)$ in the c direction changes the sign in the antiferromagnetic ordering and passes through two minima: ${}^{1c}S_{min} = -18.4$ μV/K and ${}^{2c}S_{min} = -19.2$ μV/K at ${}^{1c}T_{min} = 78.5$ K and ${}^{2c}T_{min} = 6.4$ K. The two latter minima are deeper than those in the UBi_2 case and occur at lower temperatures.

[Insert figure 8 about here]

The lowest part of the $S(T)$ data are well fitted by the equation: $S(T) = a'T + b'T^3$ being well known for the case of two components, i.e. for the diffusion and phonon-drag components in the thermoelectric power (the inset on the right hand side in figure 8). In the ordered state one should consider rather the magnon/phonon-drag component.

§ 4. Discussions and Conclusions

The temperature dependencies of the magnetic susceptibilities for UBi_2 and USb_2 single crystals reveal a similarity displaying a sharp maxima leading to the Néel temperatures of 180.8 K and 202 K, respectively. Below T_N, at about $T = 21$ K and 50 K, in the $\chi(T)$ curves of UBi_2 and USb_2 there are observed small minima (for UBi_2 see the inset of figure 1), which may result from the crystal-field effects. In UBi_2 this valley is not as deep as that observed for USb_2 or also for $UNiSb_2$ and $UPdSb_2$ there measured on the polycrystalline samples [19]. In the ordered state, when the crystal field interaction is comparable with the exchange field interaction, the anomalies in the $\chi(T)$ dependencies can occur. A crystal-field splitting (ground state is a doublet) of order of the exchange interaction yields an anomalous temperature variation of the magnetic susceptibility as was shown for CeSb and CeBi [20].

Formatted

Formatted

The electrical resistivity of UBi_2 measured along the c direction (figure 2) differs considerably from that of USb_2 (figure 5). A large hump in the resistivity curve observed in USb_2 just below T_N in the c direction can be easy explained by the fact that the corrugated

cylindrical Fermi surface in the paramagnetic state is transformed into the two cylindrical sheets in magnetically ordered state, whilst the long ellipsoidal Fermi surface changes into the two cylindrical ones [9]. In UBi_2 the Fermi surface is not rebuilt during the transition from the paramagnetic to antiferromagnetic state and such a large hump in the resistivity is not observed, but only a small hump in $\rho(T)$ occurs (figure 6b).

The genesis of six times greater resistivity anisotropy for USb_2 than that for UBi_2 (figure 3) is in the shape of the Fermi surface. The group velocity υ_g for the electronic transport defined as $\hbar^{-1}(\partial E/\partial k)$ is zero at the band extrema and zone faces (see e.g. Ref. [21]). Vector $\mathbf{v}_g = \hbar^{-1}(\partial E(\mathbf{k})/\partial \mathbf{k})$ is in the direction normal to the energy surface. This condition cannot be fulfilled along the c direction for the cylindrical surface. This means that in the ordered state of USb_2, for the c direction the group velocity of electrons should be zero. In practice, for USb_2 the cylindrical Fermi surfaces are corrugated [9] and a small component υ_g along the c-axis exists.

In a real USb_2 crystal, at low temperatures the resistivity (in relation to the electron-magnon and electron-phonon interactions) in the c direction is almost 300 times larger than that in the a direction (figure 3).

Because of a hybridisation effect with the conduction band, the 5*f*-electrons, which are responsible for existing the magnetic moment in the uranium atoms, also contribute to the electronic transport properties of UBi_2 and USb_2. They are considered to be partially localised and partially itinerant. It is known from the ^{238}U Mössbauer spectroscopy results [22] and measured large cyclotron masses, that the 5*f*-electrons in UBi_2 are more hybridised with the conduction electrons than those in USb_2 despite the larger $d_{U\text{-}U}$ distance for the former compound.

The electrical resistivity in both crystals: UBi_2 and USb_2 is satisfactorily described, below $T_N/3$, by Eq. (1), although a better fitting is obtained for a UBi_2 crystal probably due to existence of the spherical Fermi surface. In USb_2, where only cylindrical Fermi surfaces exist,

Deleted: as well as

Deleted: 2

Deleted: [11]

the best description for the ordered state is given by $\rho \sim T^{5/2}$ [7], but the mechanism yielding such a proportionality is as yet unknown.

Near the critical temperature in the *a* direction, the resistivity in USb_2 differs from that observed in UBi_2 which is firstly indicated by the temperature dependence of the derivative $d\rho/dT$. Contrary to UBi_2, the $d\rho/dT$ curve of USb_2 exhibits a peak at 202 K (the smaller inset in figure 5). Secondly, the critical exponent α in UBi_2 is negative. In UBi_2 the temperature dependence of ρ below T_N is convex while in the case of USb_2 concave (figures 6a and 6c), probably due to the different values in the energy gap on the Brillouin zone boundary. However, it should be noticed that in USb_2 the ellipsoidal (β) sheet crosses over the Brillouin zone boundary, while in UBi_2 such a case does not occur.

A metallic shape of $\rho(T)$ in the critical region, characteristic for an antiferromagnet (in agreement with classification from Ref. [16]), is revealed for both the UBi_2 and USb_2 crystals only in the *c* direction. In view of the shape of the $\rho(T)$ curve along the *a*- axis these two systems may be classified as antiferromagnetic semiconductors. This discrepancy in the classification may be caused by the fact that the authors of Ref. [16] assumed the spherical Fermi surface. In Ref. [23] it is shown that the critical behaviour of the resistivity is very sensitive to the shape of the Fermi surfaces and the position of the point of instability, Q, in the Brillouin zone.

The large-q critical spin fluctuations grow in an antifferomagnet when the temperature decreases down through T_N because the antiferromagnetic order is associated with the large-wave-vector *Q* [15]. In a metallic aniferromagnet where $Q \approx k_F$ this growth yields an increase in the resistance when the temperature is decreased through T_N. This large momentum-transfer is consistent with the conservation of energy and momentum. The temperature dependence of the resistivity of an antiferromagnetic metal, predicted in the vicinity of the critical temperature [15], is confirmed by our results especially for those obtained in UBi_2 along the *c* direction

Deleted: 9
Deleted: s
Deleted: 9
Deleted: 8
Deleted: 8

(figure 6b) and also for USb_2 (figure 6d), where, as mentioned above, a large hump in the resistivity behaviour occurs.

In conclusion, the resistivity near the critical temperature for both the UBi_2 and USb_2 crystals observed along the *a* and *c* directions varies in a manner as predicted for the energy-like behaviour [15, 16]: i.e. $\rho \sim \pm \mid t \mid^{1-\alpha}$ and then it becomes proportional to $\pm \mid t \mid^{1/2}$ close to the Ginsburg temperature, t_G, at the vicinity of a transition from the critical to mean-field behaviour.

Deleted: 8

Deleted: 9

Looking at the temperature dependencies of the thermoelectric power (figure 8) and of the resistivity (figure 5) for USb_2, both measured for the *c* direction, one sees that they have the extremes almost at the same temperature $T(\rho_{max}) \approx {}^{1c}T_{min}$. This can be explained if we take into account the fact, that in a two band model of a compensated metal the contribution of the particular band's thermoelectric power to the total thermoelectric power is weighted by the contribution of the particular band's conductivity to the total conductivity. The second minimum in the $S(T)$ dependence occurs at the temperature ${}^{2c}T_{min}$, which is close to the temperature of a maximum anisotropy ratio in the resistivity (the solid line in figure 3). This also confirms the influence of the conductivity on the thermoelectric power behaviour. Similarly for UBi_2 (figure 7), ${}^{2c}T_{min}$ is close to the temperature of a maximum anisotropy ratio of the resistivity (dashed line in figure 3).

Undoubtedly, the shape of the Fermi surface is reflected in the temperature dependence of the thermoelectric power, e.g. for USb_2, where only the cylindrical sheets exist along the *c*-axis (figure 8), the minima in $S(T)$ are more strongly pronounced than those in the case of UBi_2 (figure 7), where besides the cylindrical sheets, a spherical one was also detected. This means, that in the case when only the cylindrical Fermi surfaces exist (USb_2), the electron transport along the *c* direction due to the temperature gradient is also limited, like in the case of the

presence of the electrical field gradient. Additionally, in relation to the Umklapp processes, the electrons may drift in opposite direction to the temperature gradient.

For good quality crystals, one cannot omit the magnon/phonon-drag contribution to the total thermoelectric power at low temperatures. This contribution is visible on the $S(T)$ dependence especially along the a-axis for both the UBi_2 and USb_2 single crystals. In UBi_2 (figure 7) the small maximum ${}^{2a}S_{max}$ observed at ${}^{2a}T_{max}$ along the a-axis certainly arises from the magnon/phonon-drag effect. This thesis was confirmed in our measurements of the thermal conductivity, which will be published elsewhere, and the thermoelectric power data of two UBi_2 samples having a different purity. For the sample with a higher maximum of the thermal conductivity, a higher maximum in the thermoelectric power at ${}^{2a}T_{max}$ was observed. It is well known, that the magnon/phonon-drag effect often occurs and is large when crystals are of a high purity. Similarly for USb_2 (figure 8), in the a direction ${}^{a}S_{max}$ at ${}^{a}T_{max}$ should arise from the magnon/phonon-drag effect as well (see the left hand inset in figure 8). Obviously, this effect should exist also along the c-axis. Our calculations showed that the temperature T^* at the vicinity of which the maximum value of S_g is observed, for the a-axis, is close to the ${}^{2c}T_{min}$. This suggests that the ${}^{2c}S_{min}$ also originate from the magnon/phonon-drag effect.

Generally, the electron-magnon/phonon scattering (including normal as well as the Umklapp processes) will result in a negative magnon/phonon-drag thermoelectric power if the **q** vector of the absorbed magnon/phonon crosses an occupied region of the Brillouin zone, while S_g will be positive if the **q** vector crosses an unoccupied region of the Brillouin zone [18].

Thus, the charge transport in relation to a particular sheet of the Fermi surfaces may contribute with different magnitude and sign to the total thermoelectric power, including both the contributions: i.e. the diffusion and magnon/phonon-drag ones. Thus this gives such extremes, especially observed in USb_2 (figure 8) and in UBi_2 (figure 7) along the c direction.

Deleted: As mentioned above, the total thermoelectric power is the sum of diffusion and magnon/phonon-drag contributions. The former part can be dominant and in the c direction the latter part can be poorly visible. However in the case, when the magnon/phonon-drag is enhanced an extreme in the $S(T)$ curve is possible to occur.

Deleted: 21

In summary, the $\chi(T)$ results are similar for both compounds (figure 1) so that the magnetic properties are alike, but the transport properties at low temperatures show interesting differences particularly if measured in the *c* direction. These differences can be explained in terms of the details of the two different Fermi surfaces dictated by the different magnetic structures found in these dipnictides.

ACKNOWLEDGEMENTS

Special thanks are expressed to Prof. Z. Henkie for helpful discussion and allowing the use of his samples. The author is also grateful to Prof. R. Troć and Dr. P. Wiśniewski for their critical reading the manuscript and M.Sc. R. Gorzelniak for his help in the magnetic susceptibility measurements. The Polish Committee for Scientific Research, Grant No. 1 P03B 073 27, supported this work.

REFERENCES

[1] W. Trzebiatowski, A. Sępichowska and A. Zygmunt, Bull. Acad. Polon. Sci., Ser. Sci. Chim. **12** 687 (1964).

[2] W. Trzebiatowski and A. Zygmunt, Bull. Acad. Polon. Sci., Ser. Sci. Chim. **14** 495 (1966).

[3] J. Leciejewicz, R. Troć, A. Murasik, and A. Zygmunt, Phys. Stat. Sol. **22** 517 (1967).

[4] A. Blaise, J-M. Fournier, R. Lagnier, M. J. Mortimer, R. Schenkel, Z. Henkie and A. Wojakowski, Inst. Phys. Conf. Ser. No. 37 184 (1978).

[5] G. Amoretti, A. Blaise and J. Mulak, J. Magn. Magnet. Mat. **42** 65 (1984).

[6] Z. Henkie and Z. Kletowski, Proc. Intern. Conf. on Solid Comp. of Transition Elements, Geneve, 86-89 April (1973).

[7] Z. Henkie, Z. Kletowski, Acta Phys. Polon. **A42** 405 (1972)**.**

[8] Z. Henkie , R. Maślanka, P. Wiśniewski, R. Fabrowski and P. J. Markowski, J. J. M. Franse and M. van Sprang, J. Alloys Comp. **181** 267 (1992).

[9] D. Aoki, P. Wiśniewski, K. Miyake, N. Watanabe, Y. Inada, R. Settai, E. Yamamoto, Y. Haga and Y. Ōnuki, Philos. Mag. B **80** 1517 (2000).

[10] E. Guziewicz, T. Durakiewicz, M. T. Butterfield, C. G. Olson, J. J. Joyce, A. J. Arko, J. L. Sarrao, D. P. Moore, and L. Morales, Phys. Rev. B **69** 045102 (2004).

[11] R. Wawryk and Z. Henkie, Philos. Mag. B **81** 223 (2001).

[12] R. Troć, L. Shlyk, D. Kaczorowski, M. Potel, H. Noël, A. Pietraszko, in Landolt-Börnstein Numerical Data and Functional Relationships in Science and Technology, Group III: Condensed Matter , Vol. 27, Subvol. B 7 (Springer, 2005) p. 229.

[13] R. Troć, Z. Bukowski, C. Sułkowski, T. Plackowski, in Landolt-Börnstein Numerical Data and Functional Relationships in Science and Technology, Group III: Condensed Matter , Vol. 27, Subvol. B 7 (Springer, 2005) p. 221.

[14] R. Wawryk, Z. Henkie, T. Cichorek, C. Geibel, and F. Steglich, Phys. Stat. Sol. B **232** R4–R6 (2002).

[15] I. Balberg and A. Maman, Physica **96**B 54 (1979).

[16] S. Alexander, J. S. Helman, and I. Balberg, Phys. Rev. B **13** 304 (1976).

[17] R. Troć, Z. Bukowski, C. Sułkowski, T. Plackowski, in Landolt-Börnstein Numerical Data and Functional Relationships in Science and Technology, Group III: Condensed Matter , Vol. 27, Subvol. B 7 (Springer, 2005) p. 226.

[18] F. J. Blatt, P. A. Schroeder, C. L. Foiles, and D. Greig, Thermoelectric Power of Metals (Plenum Press, New York and London, 1976) p.p. 33, 90, 36.

[19] D. Kaczorowski, R. Kruk, J. P. Sanchez, B. Malaman, F. Wastin, Phys Rev. B **58** 9227 (1998).

[20] Y. L. Wang and B. R. Cooper, Phys. Rev. B **2** 2607 (1970).

[21] R. H. Bube, Electrons in Solids, (Academic Press, San Diego, 1988) pp. 120-121.

[22] S. Tsutsui, M. Nakada, S. Nasu, Y. Haga, D. Aoki, P. Wiśniewski, Y. Ōnuki, Phys . Rev. B **69** 054404 (2004).

[23] T. Kasuya and A. Kondo, Solid State Commun. **14** 249, 253 (1974).

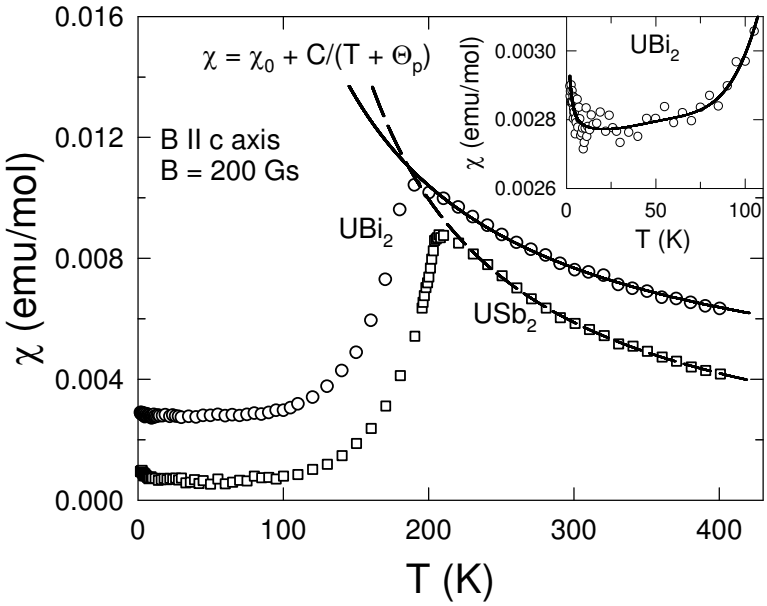

Figure 1

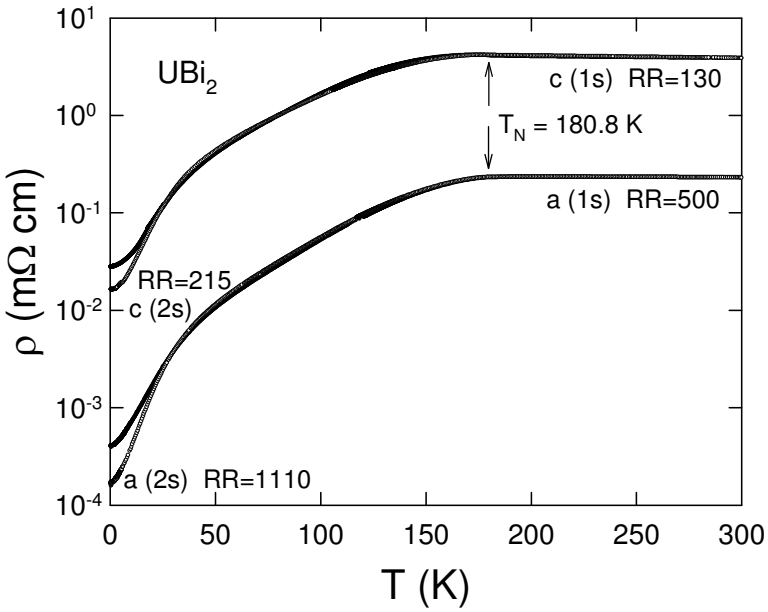

Figure 2

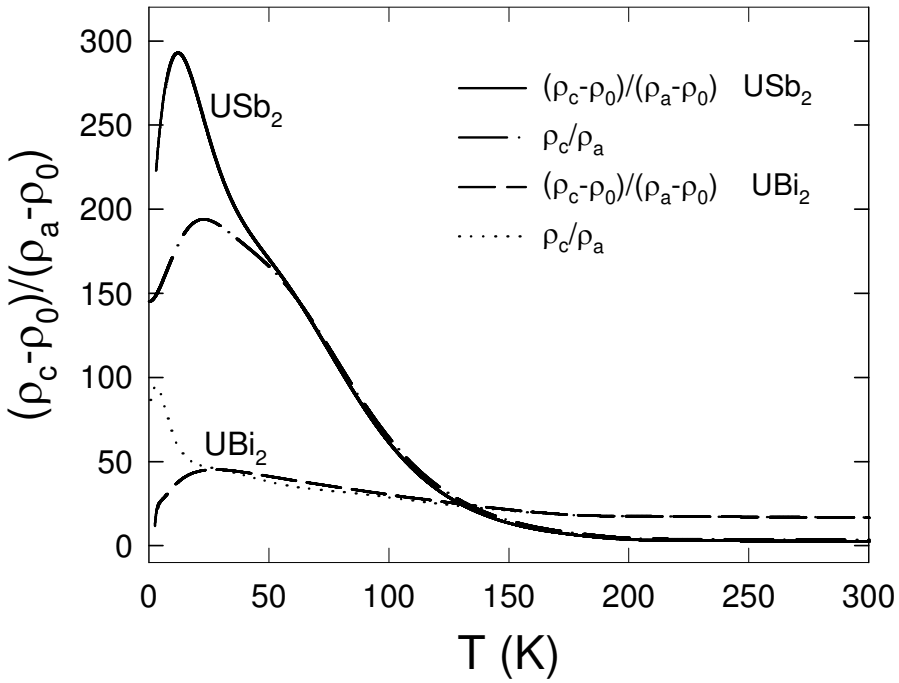

Figure 3

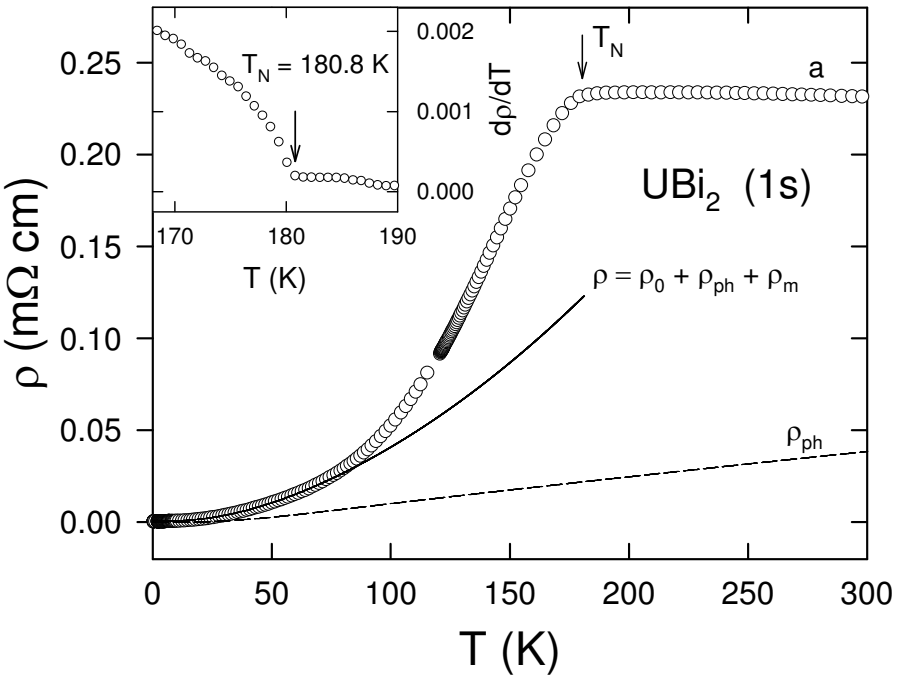

Figure 4

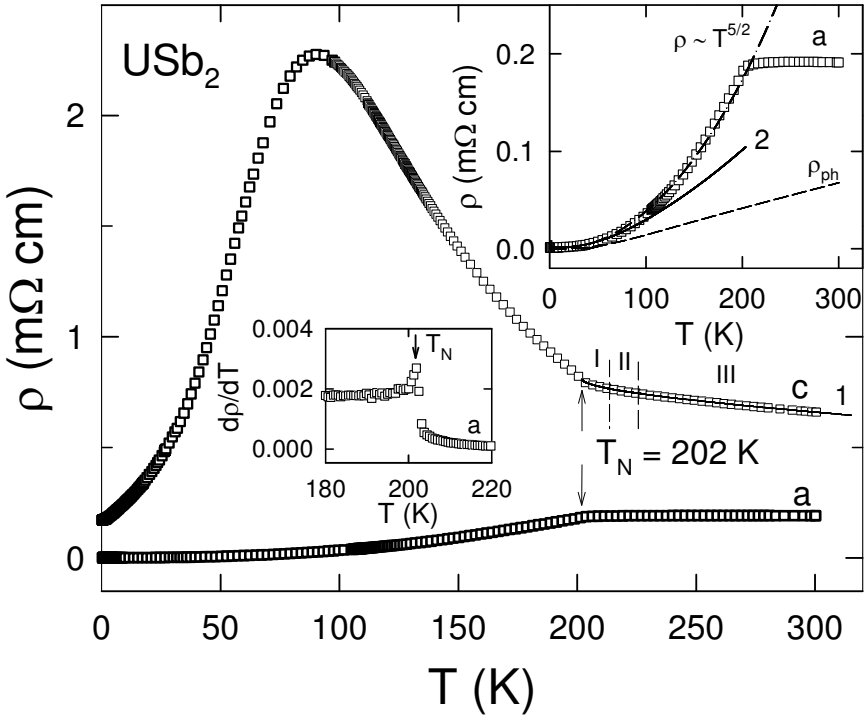

Figure 5

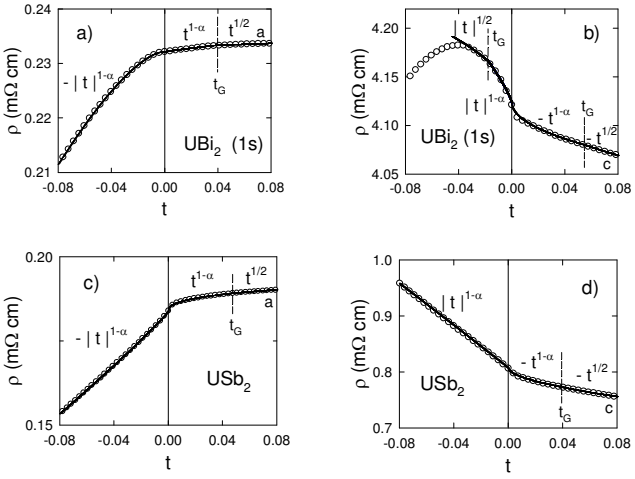
a)
b)
c)
d)
UBi2 (1s)
USb2
ρ (mΩ cm)
t
t1-α
t1/2
tG
a
c

Figure 6

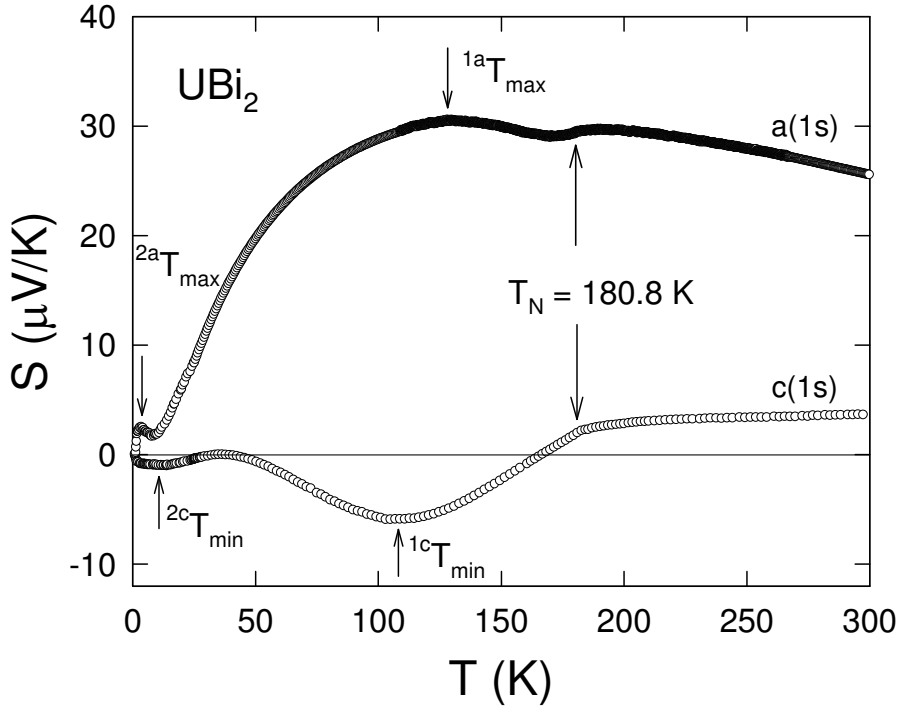
UBi2
1aTmax
a(1s)
2aTmax
TN = 180.8 K
c(1s)
2cTmin
1cTmin
S (μV/K)
T (K)

Figure 7

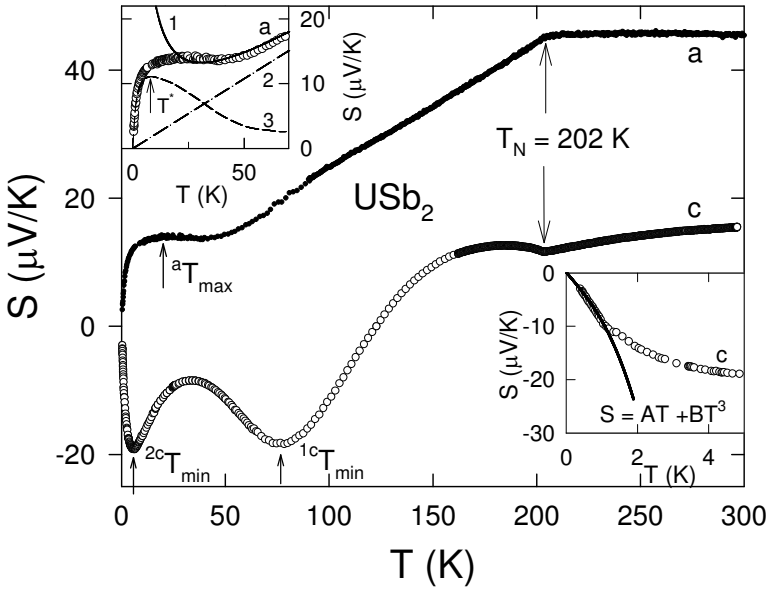

Figure 8

Figure captions

Figure 1. Magnetic susceptibility χ versus temperature of the UBi_2 (circles) and USb_2 (squares) single crystals measured in a magnetic field of 200 Gs parallel to the *c*-axis. Solid and dashed lines represent $\chi(T) = \chi_0 + C/(T + \theta_p)$ with $\chi_0 = 2.7 \times 10^{-3}$ emu/mol, Curie constant C = 1.41 emu K/mol, and θ_p = -17 K for UBi_2 and $\chi_0 = 1.42 \times 10^{-4}$ emu/mol, C = 1.38 emu K/mol, and θ_p = -59 K for USb_2. The inset displays the low temperature $\chi(T)$ data for UBi_2 (solid line is a guide for the eyes).

Figure 2. Electrical resistivity versus temperature for two UBi_2 single crystals with different purity: 1s (RR = 500 and 130) and 2s (RR = 1110 and 215) measured for the *a* and *c* crystallographic directions, respectively.

Figure 3. Temperature dependence of the anisotropy ratio $(\rho_c - \rho_0)/(\rho_a - \rho_0)$ for UBi_2 and USb_2.

Figure 4. Electrical resistivity of a UBi_2 single crystal versus temperature for the 1s sample along the *a*-axis. The solid line represents Eq. (1) with: $\rho_0 = 4.05 \times 10^{-4}$ mΩ cm, $a = 3.403 \times 10^{-2}$ mΩ cm, $b = 5.73 \times 10^{-6}$ mΩ cm, Θ =

267 K and Δ = 3.7 K. The dashed line represents the $\rho_{ph}(T)$ function (the second term in Eq. (1)). The inset shows the temperature dependence of the derivative $d\rho(T)/dT$ in units of mΩ cm K^{-1}.

Figure 5. Electrical resistivity of a USb_2 single crystal versus temperature along the *a* and *c* directions. The squares denote the experimental data. The solid line 1 represents Eq. (2) for the *c*-axis in the I part of the paramagnetic region with the following parameters: α = 0.452, A = -0.198 mΩ cm, $B = 5.506 \times 10^{-5}$ mΩ cm, and C = 0.807 mΩ cm. These parameters in the II part are: α = 0.5, A = -0.206 mΩ cm, B = 0.012 mΩ cm, and C = 0.813 mΩ cm, while in the III part: α = 0.326, A = -0.223 mΩ cm, $B = 1.553 \times 10^{-4}$ mΩ cm, and C = 0.796 mΩ cm. The inset shows the $\rho(T)$ data along the *a*-axis; the solid line 2 presents Eq. (1) with $\rho_0 = 1.178 \times 10^{-3}$ mΩ cm, $a = 8.935 \times 10^{-2}$ mΩ cm, $b = 2.025 \times 10^{-6}$ mΩ cm, Θ = 386 K, and Δ = 2.73 K; the dashed line represents $\rho_{ph}(T)$ (the second term in Eq. (1)); and the dash-dotted line displays the formula: $\rho(T) = \rho_0 + \rho_{ph} + aT^{5/2}$, where $a = 1.424 \times 10^{-7}$ mΩ cm $K^{-5/2}$. In the inset the derivative $d\rho(T)/dT$ is given in mΩ cm K^{-1} unit.

Figure 6. Electrical resistivity versus reduced temperature ($t = (T - T_N)/T_N$) along the *a* and *c* directions for a UBi_2 crystal a), b) and a USb_2 crystal c), d).

Figure 7. Thermoelectric power of the UBi_2 single crystal (1s) versus temperature measured along the *a* and *c* directions. The superscripts 1*a* and 2*a* at T_{max}, and 1*c* and 2*c* at T_{min} denote: the first and second maximum along the *a*-axis, and the first and second minimum along the *c*-axis, respectively.

Figure 8. Thermoelectric power versus temperature for USb_2 single crystal along the *a* and *c* directions. Curve 1 in the inset on the left hand side displays the equation: $S(T) = aT + b/T$ with the fitting parameters a and b equal to 0.216 μV/K^2 and 203 μV, respectively, determined along the *a*-axis. The straight line 2 and curve 3 present the diffusion and magnon/phonon-drag contributions to the total thermoelectric power, respectively. The inset on the right hand side presents the low temperature part of $S(T)$ for the *c*-axis. The solid line displays the equation: $S(T) = a'T + b'T^3$, where $a' = -7.80$ μV/K^2 and $b' = -1.36$ μV/K^4.